

Reanalysis of the Indian summer monsoon: four dimensional data assimilation of AIRS retrievals in a regional data assimilation and modeling framework

Raju Attada^{1,2} · Anant Parekh¹ · J. S. Chowdary¹ · C. Gnanaseelan¹

Received: 21 January 2017 / Accepted: 26 June 2017 / Published online: 4 July 2017
© Springer-Verlag GmbH Germany 2017

Abstract This work is the first attempt to produce a multi-year downscaled regional reanalysis of the Indian summer monsoon (ISM) using the National Centers for Environmental Prediction (NCEP) operational analyses and Atmospheric Infrared Sounder (AIRS) version 5 temperature and moisture retrievals in a regional model. Reanalysis of nine monsoon seasons (2003–2011) are produced in two parallel setups. The first set of experiments simply downscale the original NCEP operational analyses, whilst the second one assimilates the AIRS temperature and moisture profiles. The results show better representation of the key monsoon features such as low level jet, tropical easterly jet, subtropical westerly jet, monsoon trough and the spatial pattern of precipitation when AIRS profiles are assimilated (compared to those without AIRS data assimilation). The distribution of temperature, moisture and meridional gradients of dynamical and thermodynamical fields over the monsoon region are better represented in the reanalysis that assimilates AIRS profiles. The change induced by AIRS data on the moist and thermodynamic conditions results in more realistic rendering of the vertical shear associated with the monsoon, which in turn leads to a proper moisture transport and the moist convective feedback. This feedback benefits the representation of the regional monsoon characteristics, the monsoon dynamics and the moist convective processes on the seasonal time scale. This study

emphasizes the use of AIRS soundings for downscaling of ISM representation in a regional reanalysis.

Keywords Indian summer monsoon · Four dimensional data assimilation · AIRS profiles · Regional model

1 Introduction

The Indian summer monsoon (ISM), apart from being complex weather pattern, is also one of the most important components of the global atmospheric general circulation system. It plays a key role in modulating the weather and climate in many parts of the globe (e.g. Lau et al. 2000). Furthermore, the Indian economy is driven primarily by the agriculture sector that is solely conditioned and controlled by the ISM performance (Gadgil and Gadgil 2006). Precipitation and circulation processes associated with the ISM intimately re-enforce each other, i.e. the moist thermodynamic processes play a vital role in the ISM performance and its characteristics. Krishnamurti and Bhalme (1976a) reported that the vertical structure of temperature associated with ISM has a coherent response to precipitation strength in the middle and lower troposphere, while the vertical structure of water vapour is important for lower to mid-troposphere instability, mid-troposphere heating and circulation. This feedback process is inadequate in many global and regional climate models. Hence, proper representation of the vertical structure of temperature and moisture is one of the basic requirements for the climate models (e.g. Liang et al. 2012) to represent ISM. Otkin (2012) suggested that an accurate forecast of cloud cover and precipitation is more likely to occur when the spatial distribution of temperature and water vapour is accurately specified in the models. Several studies have pointed out

✉ Raju Attada
rajuattada@gmail.com

¹ Theoretical Studies Division, Indian Institute of Tropical Meteorology, Pune 411 008, India

² Present Address: King Abdullah University of Science and Technology, Thuwal, Saudi Arabia

that the accurate initialization of high resolution temperature and moisture profiles are important for improving the model physics and associated precipitation processes (e.g. Susskind et al. 2003; Davolio and Buzzi 2004; Fan and Tilley 2005; Li and Liu 2009; Rakesh et al. 2010; Miyoshi and Kunii 2012; Singh et al. 2012). Raju et al. (2015a) carried out a detailed assessment of the Weather Research and Forecasting (WRF) model and found that it could successfully represent monsoon elements and convective precipitation zones over the ISM region with some overestimation. They also reported that the overestimation is due to strong easterly wind bias, which brings excess moisture from the western Pacific Ocean and Bay of Bengal (BoB) to the monsoon core region (MCR). In addition, it is reported that the vertical baroclinic response of temperature is weaker in the model compared to the observations, thereby raising key questions about the representation of moist thermodynamic processes in the monsoon region.

Fundamentally, the vertical profiles of temperature and water vapour are poorly sampled by in situ observations. Hence this deficiency propels the difficulty in modelling the temperature and moisture fields and the requirement of accurate initial conditions (e.g. Raymond et al. 2004). Recent advancements in remote sensing techniques are beginning to address this issue. One such advancement is the advent of Atmospheric Infrared Sounder (AIRS) instrument on board the Aqua satellite, which provides temperature and water vapour mixing ratio (WVMR) profiles in clear to partly cloudy conditions from near surface into the stratosphere (Aumann et al. 2003; Susskind et al. 2006; Reale et al. 2012) with high vertical resolution and accuracy. McNally and Watts (2003) showed that AIRS measurements can improve the prediction of sensible weather elements within a regional model. Le Marshall et al. (2006) found a positive impact on the National Centers for Environmental Prediction (NCEP) operational system's forecasting skill resulting from the assimilation of AIRS profiles. Xavier et al. (2008) showed that inclusion of temperature and humidity profiles in the model through a nudging technique improves the representation of low-pressure systems during ISM. Singh et al. (2008, 2010, 2012) assimilated AIRS retrieved profiles in the WRF model and showed that AIRS data has significant impact on the precipitation forecast of different weather systems. Zhou et al. (2010) reported that the assimilation of AIRS profiles substantially improves precipitation analyses in global data assimilation and forecast systems. AIRS profiles can also enhance the characterization of the thermodynamic environment leading to a more accurate precipitation forecast (Zavodsky et al. 2012). Later, Reale et al. (2012) showed increment in the global forecast skill by assimilating AIRS temperature profiles. They also achieved considerable progress in analysis as well as

forecast of a major precipitation event over the Indus River Valley up to 7 days. Recently, Raju et al. (2014, 2015c) demonstrated significant impact of AIRS temperature profiles assimilation on ISM circulation characteristics. However, the impact of assimilating both temperature and moisture profiles together has not been explored with the WRF model for ISM and this is exactly what this paper envisages to undertake.

The paper is organized as follows. Section 2 gives a detailed description of the model, experimental set up, various data sets and methodology. The impact of AIRS profiles on model reanalyzed atmospheric states is discussed in Sect. 3; Sect. 4 explains the possible physical mechanisms, while summary and concluding remarks are provided in Sect. 5.

2 Model, data assimilation and methodology

2.1 Model

The WRF model version 3.2.1 (Skamarock et al. 2008) is used for monsoon representation for the period of 2003–2011. This model is a limited area, non hydrostatic primitive equation model with multiple options for different physical parameterization schemes. It is designed to be a flexible, state-of-the-art atmospheric model system that is portable and efficient on available parallel computing platforms. It is suitable for use in a broad range of applications across the scales ranging from meters to thousands of kilometers. The zonal extent of the model domain is from 30°E to 180°E and the meridional extent is from 30°S to 40°N (370 by 198 grid points). The model has a spatial resolution of 45 km and 40 vertical levels, the highest of which is located at 50 hPa.

2.2 Data Assimilation

Four dimensional data assimilation (FDDA) technique is used in the present study for the assimilation of temperature and moisture profiles of AIRS. The FDDA is a continuous data assimilation method that relaxes the model state towards the observed state (Stauffer and Seaman 1990, 1994). Fundamentally, this methodology has its roots in control theory where an empirical forecast error term is added to the dynamical constraint, essentially a feedback control added to the dynamics (e.g. Stauffer et al. 1991; Lakshmivaran and Lewis 2011). This method balances the initial conditions fields geostrophically and hydrostatically when they are integrated forward. In the analysis, Newtonian relaxation term is added to the prognostic equations for temperature and moisture using the following equation,

$$\frac{\partial \alpha}{\partial t} = F(\alpha, X, t) + G W_s W_t \varepsilon (T, x)(y^o - H\alpha) \quad (1)$$

where ‘ α ’ is a prognostic variable, F denotes the normal tendency terms due to physics, advection, etc. X represents independent spatial variables and t is time. y^o is the observation vector, H is the operator that projects model forecast to the observation grid, G is the nudging magnitude matrix, and W_s , W_t are the spatial and temporal nudging (weighting) coefficients, which are used to map the innovation in observation space and time to the model grid cell and time step. The weighting function for W_s is obtained based on Cressman (1959) and for W_t is based on Stauffer and Seaman (1990). The radius of influence (time window) is considered to be about 100 km (12 h). The nudging strength is $3 \times 10^{-4} \text{ s}^{-1}$ (e.g. Stauffer and Seaman 1994) and ε denotes observation quality factor. It is important to mention that the specification of nudging strength is very sensitive in the model. Stauffer and Seaman (1990, 1994), Stauffer et al. (1991), Fast (1995), Seaman et al. (1995) did many sensitivity experiments and reported that the nudging strength of $3 \times 10^{-4} \text{ s}^{-1}$ works better. Raju et al. (2014, 2015c) also supported that this choice of nudging coefficient is efficient for monsoon representation in WRF.

Each observation is ingested into the model at its observed time and location with proper space–time weights and the model spreads the information in time and space according to the model dynamics. The FDDA modifies the model temperature and moisture profile at every time step, according to the difference between observed and forecasted and attempts to bring the forecast as close as possible to reality. The set of differences between the model and observed state is computed at the observational locations and analyzed back to the grid. Thus, the model equations assure a dynamical consistency while the observations keep the model close to the true conditions and make up for errors and gaps in the initial analysis and deficiencies in the model physics. This method has several advantages; first, it is computationally efficient, simple and robust. Secondly, it allows the model to ingest data continuously rather than intermittently, with the full model dynamics. A study by Leslie et al. (1998) reported that the impact of FDDA is similar to that of four dimensional variational systems, which is computationally intensive and expensive.

2.3 Data and Methodology

2.3.1 Initial conditions and boundary forcing

NCEP operational analyses regridded at $1^\circ \times 1^\circ$ at every 6 h are used to determine the initial and boundary conditions for downscaling experiments. This data has been considered because the observed vertical profiles of temperature and

water vapor over the Indian region used in this analysis are much less. As suggested by Zavodsky et al. (2012), NCEP does not contain sufficient information about the vertical structure of temperature and moisture, thereby limiting their potential impact on analyses. Therefore, assimilation of AIRS profiles of temperature and WVMR on NCEP operational analyses will incorporate the impact. The daily sea surface temperature (SST, Thiebaut et al. 2003) is used as the slowly varying lower boundary condition for the model.

2.3.2 AIRS

AIRS has 2378 infrared channels and four channels in visible and near-infrared. It has provided unprecedented three dimensional distributions of temperature and moisture at a global scale, with very high spatio-temporal resolutions (e.g. Parkinson 2003; Fu et al. 2006; Tian et al. 2006; Wong et al. 2011) over both land and ocean. It has been proven to be beneficial in identifying the fine thermal and moisture structure of the atmosphere in a number of studies (e.g. Wong et al. 2011). Recent release of AIRS V6 data is covering neural network training based on the European Centre for Medium-Range Weather Forecasts (ECMWF), whereas AIRS (Level-3, version-5) is independent and generate level-by-level error estimates $\delta T(p)$ for retrieved quantities, which is used as estimates for quality control. Since the present study is focused on how independent profiles of temperature and moisture can impact the ISM structure and the associated process, AIRS Version 5 products based on retrieval algorithm by Susskind and Reale (2009) are used. The AIRS data has a twice-daily temporal resolution and spatial resolution of 45 km. The temperature (moisture) profiles are available at 24 (12) standard pressure levels between 1000 and 1 hPa (1000–100 hPa). This product is the most accurate and stable set of hyper-spectral infrared measurements made in space to date and provides daily temperature (moisture) profiles at an accuracy 1 K per 1 km (15% in 2 km). The details on AIRS observations (vertical resolution and uncertainties) are described by Aumann et al. (2003). The temperature and WVMR profiles are validated for both land and ocean for a broad range of geographic conditions (Divakarla et al. 2006; Tobin et al. 2006). These data are continuously assimilated during model integration. Prior to data assimilation, all data underwent a rigorous quality control.

2.3.3 Experiment set up and validation

The model set up is similar to Raju et al. (2015a, b). The model is integrated from 1st May to 1st October for every year during the study period. The representation corresponding to June to September (JJAS) is used in the present study, allowing 1 month as a model spin up time. One month spin

up time is sufficient for the dynamical equilibrium between the lateral forcing and the internal physical dynamics of the model (Anthes et al. 1989). In summary CTRL and assimilated experiments (TQEXP) represent two downscaled reanalyses, forced by NCEP boundary conditions and daily varying SSTs, with the additional assimilation of AIRS temperature and moisture profiles being performed in the TQEXP. Therefore, any difference in the representation of the ISM circulation and structure between the CTRL and TQEXP can be attributed to the information content of AIRS retrievals. For the validation, the ECMWF Interim reanalysis (ERA-Interim) data available at a spectral resolution of T255 (approximately $0.7^\circ \times 0.7^\circ$, Dee et al. 2011) are used during the study period. It is the latest global atmospheric reanalysis product with highest accuracy (Lin et al. 2014). Over land and ocean, daily precipitation estimates provided by the Global Precipitation Climatology Project (GPCP) at $1^\circ \times 1^\circ$ resolution (Huffman et al. 2001) and Tropical Rainfall Measuring Mission (TRMM) daily precipitation (3B42V6; Huffman et al. 2007) data available at $0.25^\circ \times 0.25^\circ$ are used.

For the quantitative assessment of representation in TQEXP compared to CTRL, the statistical scores such as bias and root mean square error (RMSE) are computed. In addition, the equitable threat score (ETS) and bias score (BS) are estimated for rainfall, which is a metric to measure the model's ability of categorical rainfall forecast (Anthes et al. 1989). Pattern correlation (PC) over the domain is estimated for large spatial scale comparative assessment of reanalyzed mean fields with the observed fields.

Furthermore, to understand the thermodynamical response, moist static energy (MSE, which is a useful measure of vertical instability) is estimated using following equation:

$$MSE = C_p T + gZ + Lq \quad (2)$$

where T is air temperature, C_p is the specific heat of air at constant pressure, Z is height, g is gravitational acceleration, L is the latent heat of vaporization at 0°C , and q is the specific humidity. Precipitable water content (PW) in an air column is calculated as follow:

$$PW = \frac{1}{g} \int_{P_t}^{P_s} q dp \quad (3)$$

where P_s is surface pressure and P_t is pressure at top of the air column.

In order to quantify the skill of reanalyzed atmospheric fields due to assimilation of AIRS profiles, Forecast Impact (FI) parameter is computed (Wilks 2006) using Eq. (4).

$$FI = \left[1 - \frac{RMSE_E}{RMSE_C} \right] \times 100\% \quad (4)$$

where, $RMSE_C$ ($RMSE_E$) is error with respect to observations for the prognostic variable from CTRL (TQEXP). The positive (negative) value of FI indicates a reduction (increase) of error in TQEXP with respect to CTRL. All the FI scores discussed in this study are significant at 95% confidence level following Student's *t* test.

3 Results

3.1 Impact of AIRS profiles on reanalysed circulation and moist thermodynamic fields

Spatial distributions of the FI score for low level (850 hPa) and upper level (200 hPa) winds in TQEXP are presented in Fig. 1. FI for low level zonal wind (Fig. 1a) shows significant positive values over the entire monsoon region. The highest positive FI score is observed in important regions such as the Somali coast (about 90%), the Madagascar high and the monsoon trough region (about 85%). In case of upper level zonal winds (Fig. 1b), FI is positive over the Indian subcontinent, west Pacific and over the Arabian Peninsula. It is also observed that FI over the central equatorial Indian Ocean shows a marginal benefit in TQEXP (30–50%) over CTRL in the upper tropospheric zonal winds. Furthermore, FI for the lower and upper level meridional winds are shown in Fig. 1c, d. The significant positive values of low level meridional winds over Indian region, the Western Ghats and southwest Indian Ocean are evident; however negative FI (about 10–15%) is noted over the Tibetan region. On the other hand, FI for upper level meridional winds is positive over most of the oceanic regions. Overall, the representation of the monsoon circulation is better in TQEXP compared to CTRL.

Fundamentally, the monsoon system is forced by land-sea thermal contrast and meridional tropospheric temperature gradients. Therefore, FI is also estimated for low and mid tropospheric temperature (Fig. 2a, b). The positive FI is noted over the entire oceanic region and the Indian subcontinent. However, negative FI values (30–50%) are found over the west Pacific and Arabian Peninsula coast for lower tropospheric temperature. Mid tropospheric temperatures display positive FI over the entire Indian Ocean and Tibetan region, which are dominant heat sources of monsoon. Lower tropospheric WVMR (vertically integrated from surface to 850 hPa) distribution is closer to the observations over the oceanic region (Fig. 2c) in TQEXP than CTRL. FI for the upper troposphere (averaged between 400 and 200 hPa) has shown a ratio of 0.4 between the errors and the FI score is 60% over the Indian subcontinent region and southern oceanic region compared to CTRL. This analysis supports that assimilation of AIRS profiles increases

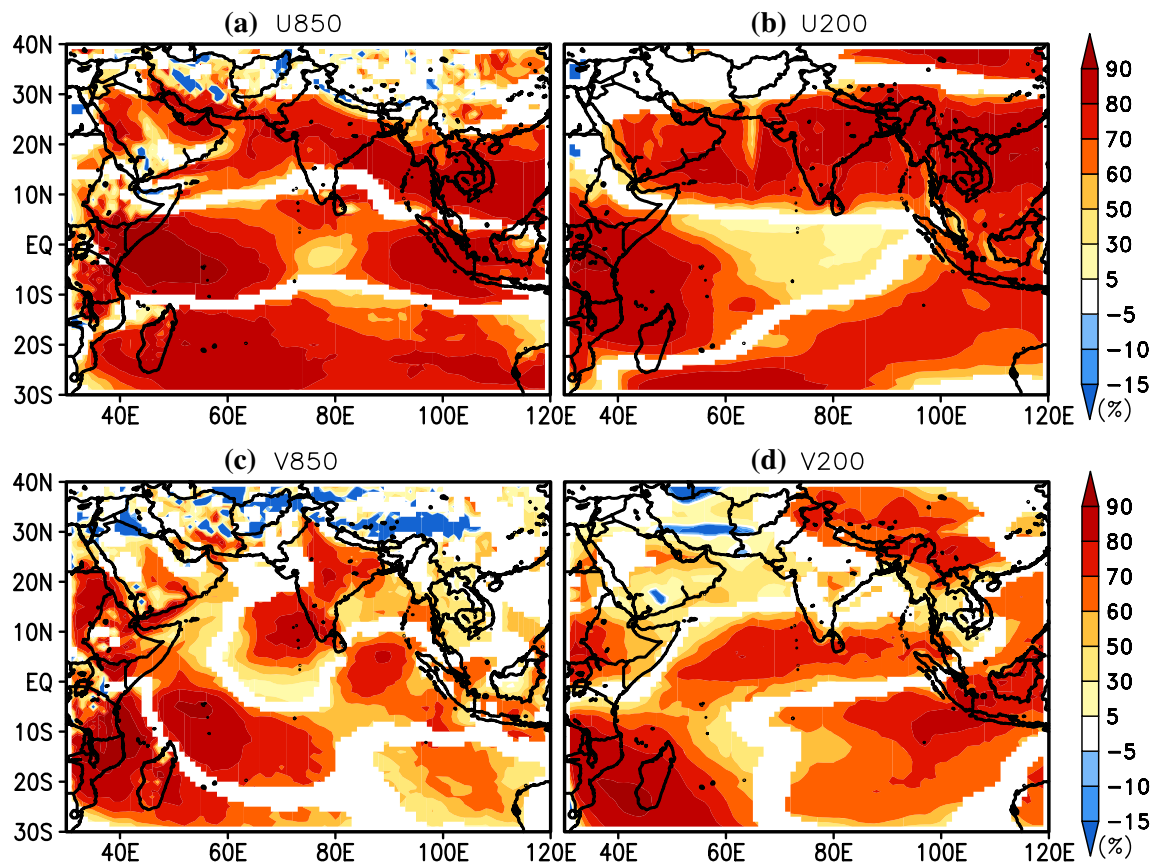


Fig. 1 Spatial distribution of Forecast Impact score for (a, c) low level and (b, d) upper level zonal and meridional winds in TQEXP over CTRL

the model skill for moisture and temperature fields during the monsoon season.

3.2 Spatial distribution of seasonal mean monsoon features

Spatial distribution of seasonal mean sea level pressure (SLP) and midtropospheric temperature from CTRL, ERAI and TQEXP are shown in Fig. 3. CTRL (Fig. 3a), ERAI (Fig. 3b) and TQEXP (Fig. 3c) produced the meridional gradient of SLP, the geographical location of surface heat low and the position of the monsoon trough reasonably well. However, the southward extension of 1008 hPa isobar is noted in CTRL compared to ERAI, indicating the underestimation (overestimation) of SLP over the Indian Ocean (north of 25°N) in CTRL. This asymmetry in SLP bias suggests that the model suffers from a weak meridional SLP gradient. CTRL shows (Fig. 3d) large positive bias (4.7 hPa) and RMSE (6.9 hPa), whereas TQEXP (Fig. 3e) shows, weak negative bias (−2.2 hPa) and RMSE (4.2 hPa) over the study area. PC of SLP distribution in TQEXP (CTRL) with ERAI is 0.94 (0.79). This confirms that TQEXP could capture better spatial distribution of

SLP than CTRL, supporting better low level monsoon circulation in TQEXP. In addition to that, CTRL and TQEXP are able to represent mid-troposphere temperature features over the Tibetan plateau as well as meridional temperature gradient as in ERAI with higher PC in TQEXP than CTRL (Table 1). Figure 3f shows the temporal evolution of tropospheric temperature (averaged between 700 hPa and 200 hPa) gradient (TTG, Xavier et al. 2007) between 40°E–100°E; 5°N–35°N and 40°E–100°E; 15°S–5°N from CTRL, TQEXP and ERAI. ERAI shows higher TTG (corresponding to higher latent heat release) during the peak monsoon season compared to that of onset and withdrawal phase of the monsoon. TTG is underestimated in CTRL compared to ERAI whereas TQEXP produced a better temporal evolution of TTG. The above analysis confirms that large scale thermal contrast associated with the ISM is well represented in TQEXP as in the observations.

Lower troposphere circulation displays strong easterly winds south of equator extended up to 30°S and broader LLJ with south eastward shift in the core along the Somali coast in CTRL (Fig. 4a, c). Joseph and Sijikumar (2004) suggested that the axis of LLJ can get oriented south eastward when the convective heating of the

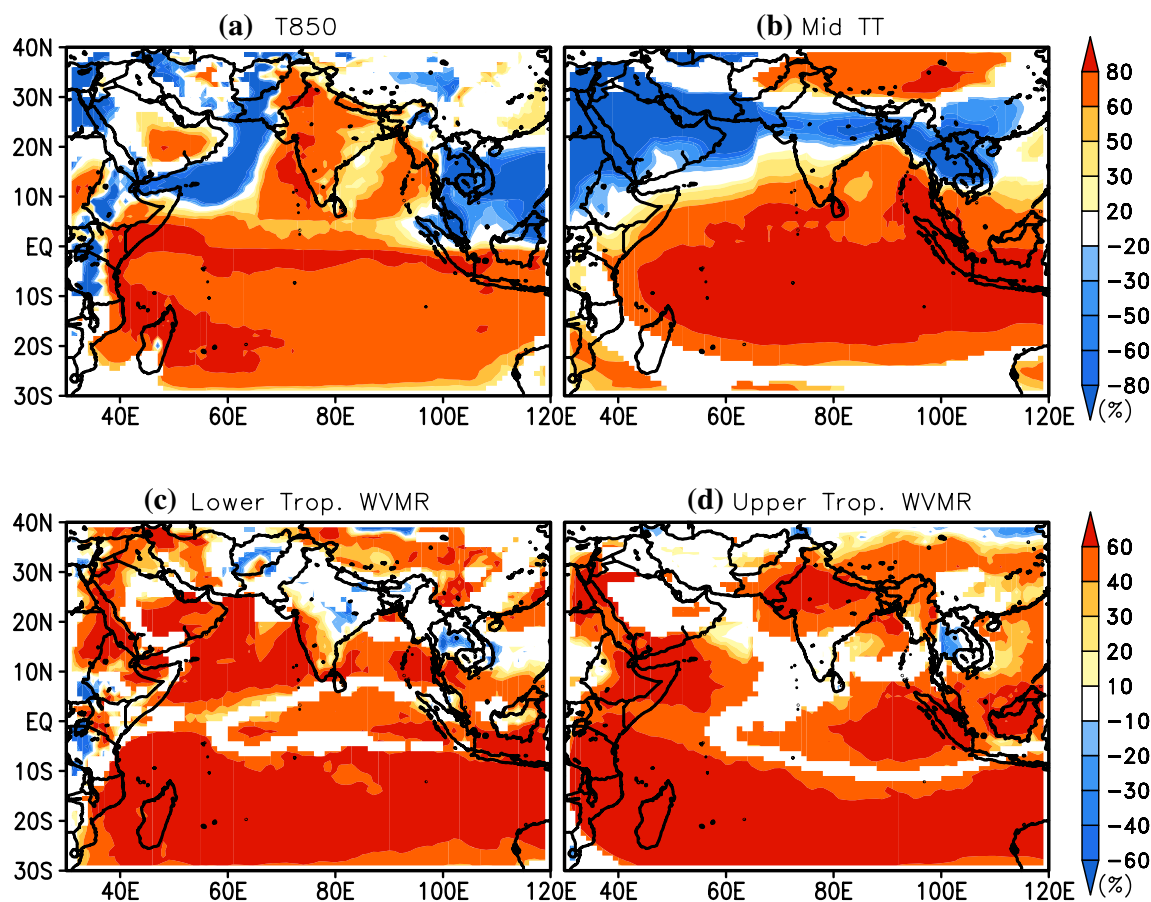


Fig. 2 Spatial distribution of Forecast Impact score for **a** lower troposphere temperature, **b** midtroposphere temperature, **c** lower troposphere WVMR and **d** upper troposphere WVMR in TQEXP over CTRL

atmosphere is placed at low latitude of the Indian Ocean, which is also the case in CTRL (Fig. 4a). The easterly (westerly) bias over the western Pacific to MCR (east coast of Africa) is mainly due to the unrealistic zonal pressure gradient in the model which is consistent with Raju et al. (2015a). On the other hand, in the case of TQEXP (Fig. 4b) LLJ and cyclonic circulation over BoB are well structured. The strong easterly winds over south of the equator is better in TQEXP compared to the CTRL. In turn TQEXP could enhance the PC for low level monsoon circulation with ERAI compared to CTRL (Table 1). Upper tropospheric (200 hPa) wind distribution from CTRL, ERAI and TQEXP is shown in Fig. 4d–f. CTRL (Fig. 4d) represented the upper tropospheric circulation features such as Tibetan anticyclone, tropical easterly jet (TEJ) and subtropical westerly jet (SWJ) in agreement with ERAI. However, Tibetan anticyclonic circulation in the CTRL is located south of its normal position and the northward extension of TEJ is confined to 15°N, whereas it is extended up to 25°N in ERAI. The maximum wind speed of TEJ is located to the west of the southern tip of

India in ERAI (Fig. 4f), whereas in CTRL it is extended up to the east coast of Africa. On the other hand, TQEXP (Fig. 4e) captured the proper location of Tibetan anticyclone, spatial extent of TEJ and SWJ. It indicates that accurate representations of thermal structure in mid to upper level are achieved through the inclusion of the AIRS profiles. However, TEJ is found to be weaker in the TQEXP than CTRL. It may be due to a mismatch between thermal winds from the assimilated temperatures and the winds. Krishnamurti et al. (2005) suggested that the thermal wind and the pressure gradients are always weaker than the observed winds for the case of super geostrophic winds in the model. Hence it causes weaker upper level winds compared to observations in assimilation experiment. During the monsoon strong easterly in upper troposphere and westerly in lower troposphere produces easterly wind shear over the monsoon region, CTRL and TQEXP represent easterly wind shear (Fig. 5a, b), however geographical position (zonal distribution) and strength of the shear in TQEXP (Fig. 5b) is in close agreement with ERAI (Fig. 5c). PC for the wind shear

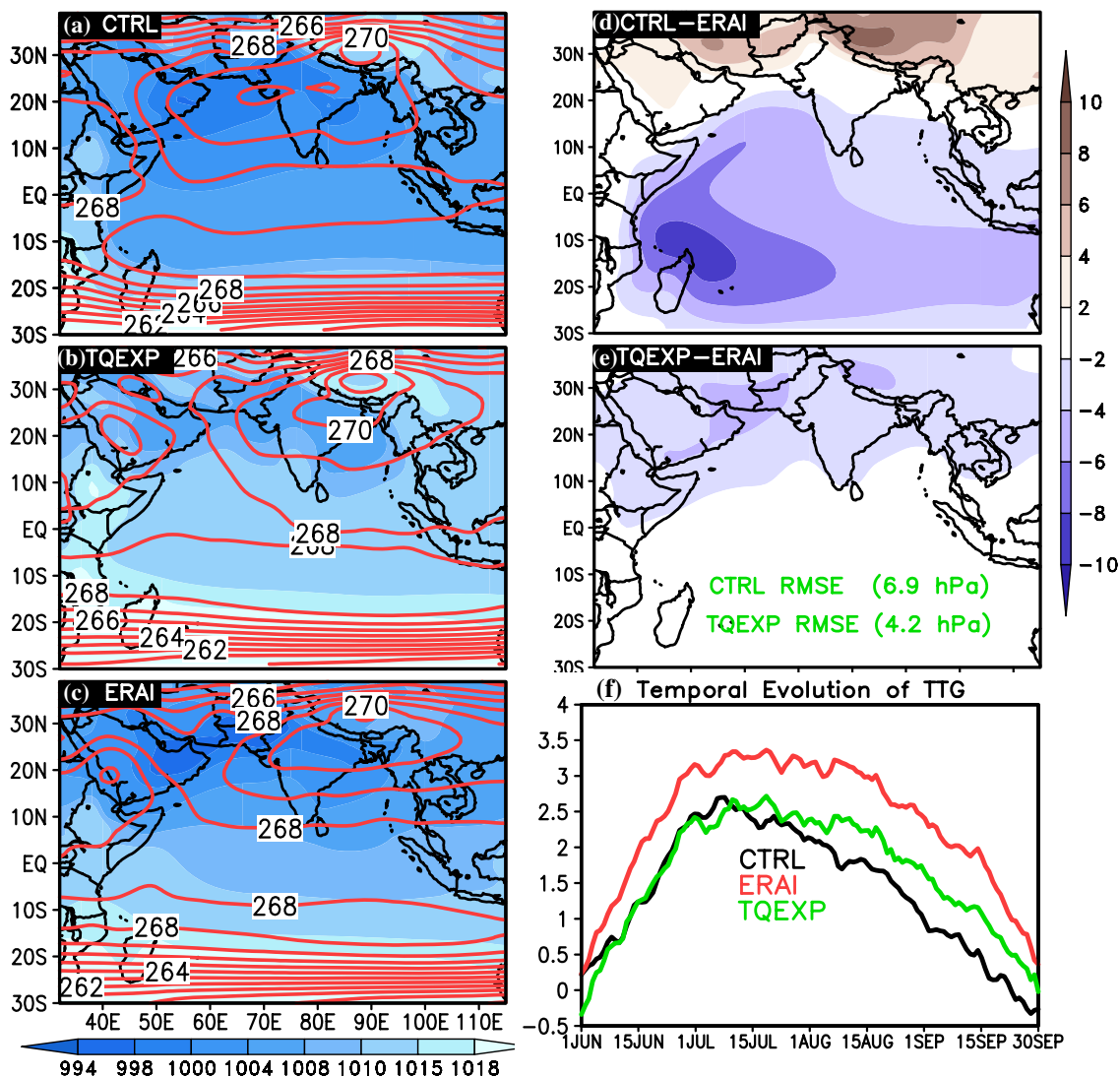


Fig. 3 JJAS mean spatial distribution of SLP (hPa, shaded) overlaid with 500 hPa temperature (K, contours) (a–c) and corresponding SLP (hPa) bias against ERAI (d, e). The temporal evolution of meridional tropospheric temperature gradient (K) during monsoon (f)

Table 1 Pattern correlation for various fields between CTRL and ERAI/GPCP; TQEXP and ERAI/GPCP during 2003–2011

CTRL vs ERAI/ GPCP	Variable	TQEXP vs ERAI
0.79	SLP	0.94
0.89	Midtropospheric temperature	0.96
0.73	Low level winds	0.97
0.81	Upper level winds	0.99
0.42	Rainfall	0.76
0.7	Vertical wind shear	0.9

is higher in TQEXP (0.9) than CTRL (0.7) compared to ERAI. Recently, Reale et al. (2017) showed that small errors in the vertical shear of wind over the Indian Ocean

could lead to large errors in the atmospheric dynamics, which eventually can feedback to the associated convective activities. Overall, the analysis indicates that proper temperature and WVMR distribution in the model can be useful for realistic representation of the easterly wind shear and monsoon convective systems.

Hence, it is now important to examine whether these developments are translated into the seasonal rainfall distribution or not. Figure 5d–f shows the seasonal mean rainfall over the ISM region from CTRL, TQEXP and GPCP respectively. The CTRL is able to capture the major convective centres over the eastern Arabian Sea (AS), BoB, MCR and South China sea as in the observations. However, rainfall is overestimated over the AS, BoB, and southwest Indian Ocean regions. Unrealistic

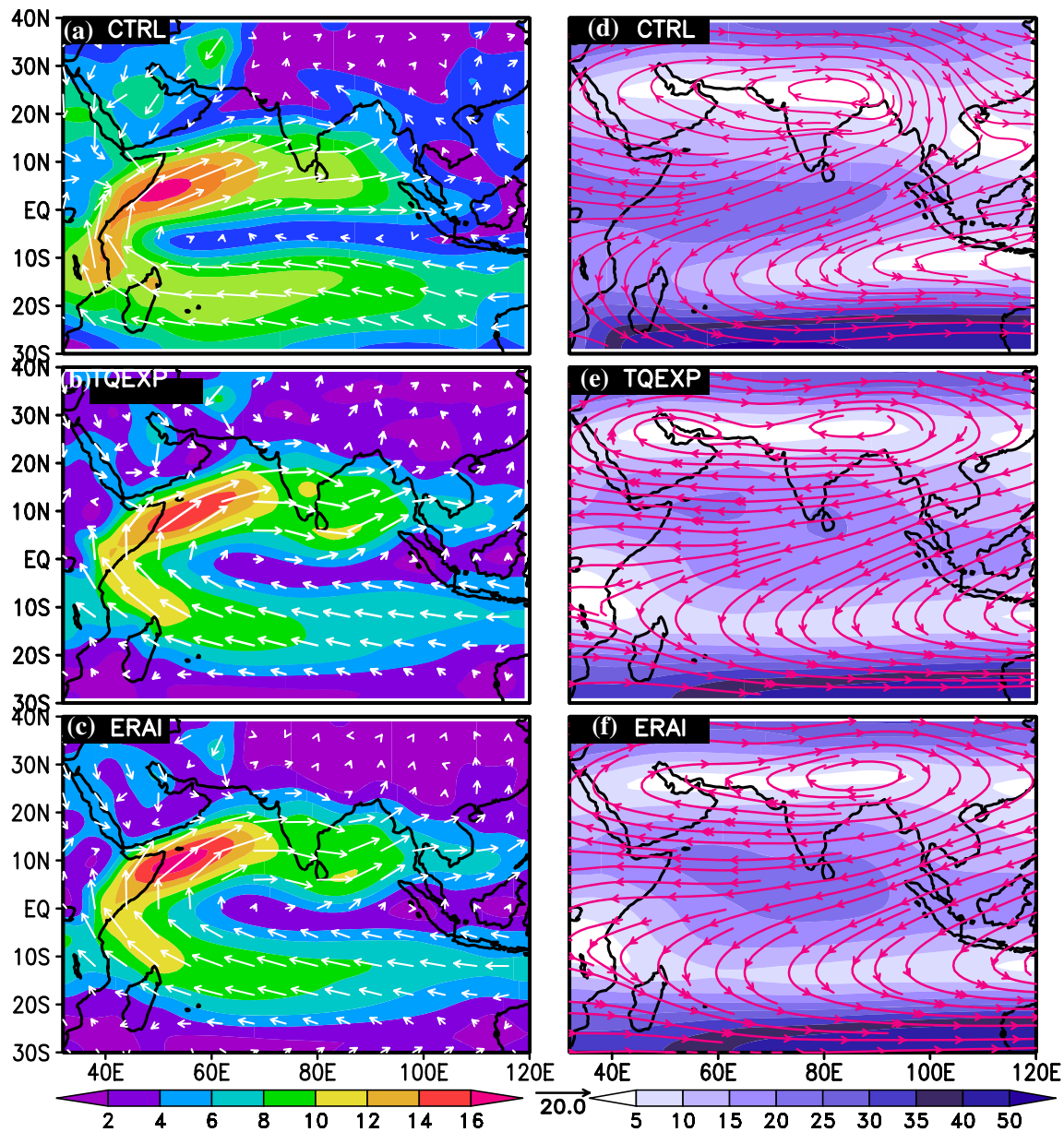


Fig. 4 JJAS mean spatial distribution of low level (850 hPa) winds (**a–c**, ms^{-1} , vectors) and upper level (200 hPa) winds (**d–f**, ms^{-1} , stream lines) respectively from CTRL, ERAI, TQEXP. Wind speeds are shaded

double inter tropical convergence zone (ITCZ) like rainfall pattern is evident in CTRL over the tropical Indian Ocean regions. Such unrealistic double ITCZ like rainfall pattern is disappeared in TQEXP, which is one of the major achievements with the assimilation of AIRS profiles. The PC for precipitation is higher in TQEXP than CTRL (Table 1). It is important to note that precipitation distribution is near realistic over the Indian land region, but overestimated over the oceanic regions.

To diagnose the role of various components of monsoon for the rainfall biases in CTRL and reduction of biases in TQEXP are explored. Seasonal mean meridional

distribution of easterly wind shear, lower tropospheric specific humidity (averaged from surface to 850 hPa), TTG (averaged between 600 and 200 hPa) and equivalent potential temperature (EPT) (averaged between 1000 and 850 hPa) associated with the ISM are shown in Fig. 6 from CTRL, ERAI and TQEXP. The meridional distribution of easterly shear (averaged between 65°E and 95°E during JJAS), which is one of the key parameters for the northward propagation of the convection (e.g. Jiang et al. 2004; Abhik et al. 2014) is underestimated over the southern latitudes (ocean) and overestimated over northern latitudes (land) in CTRL (Fig. 6a). The weaker gradient of integrated

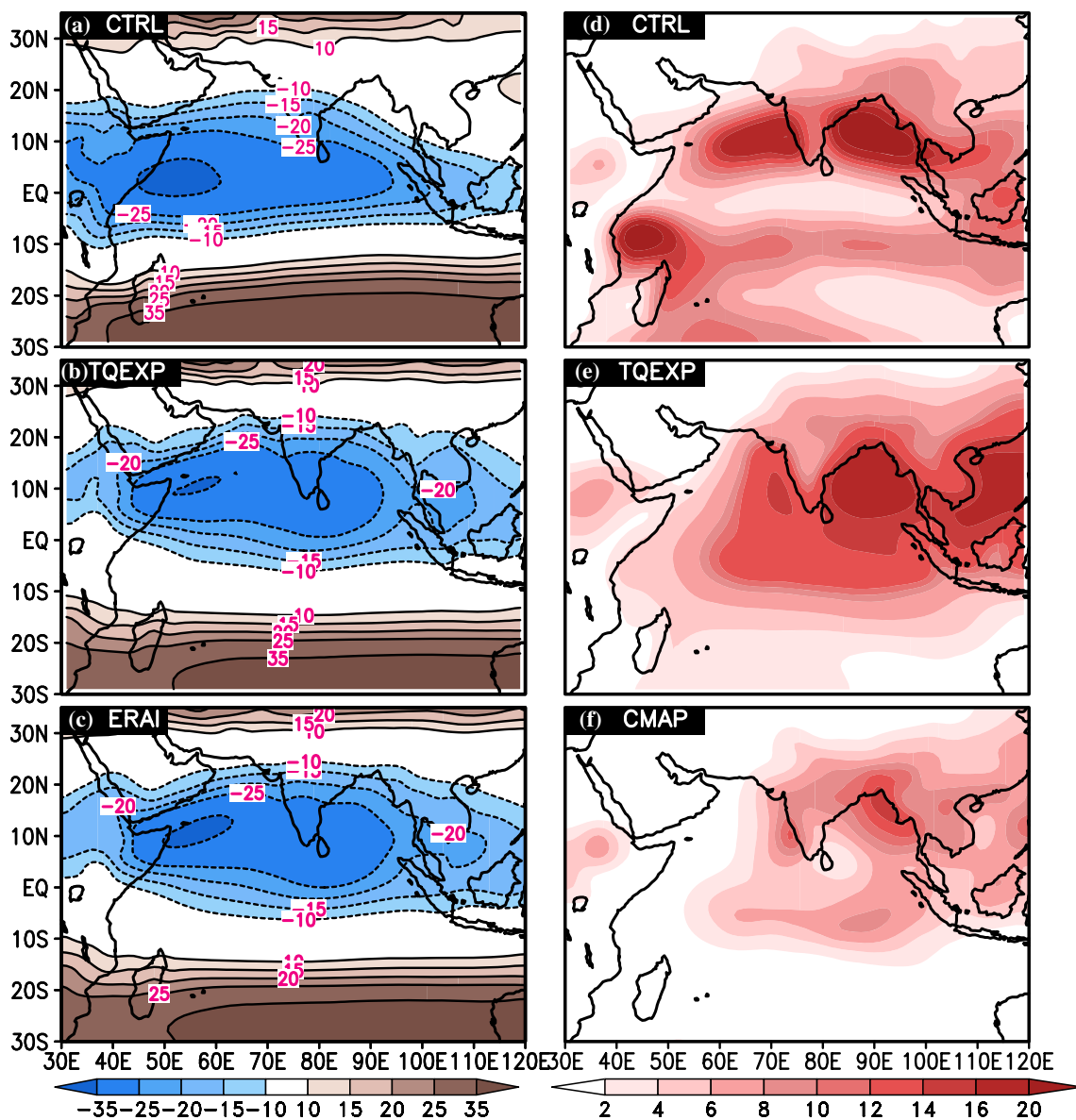


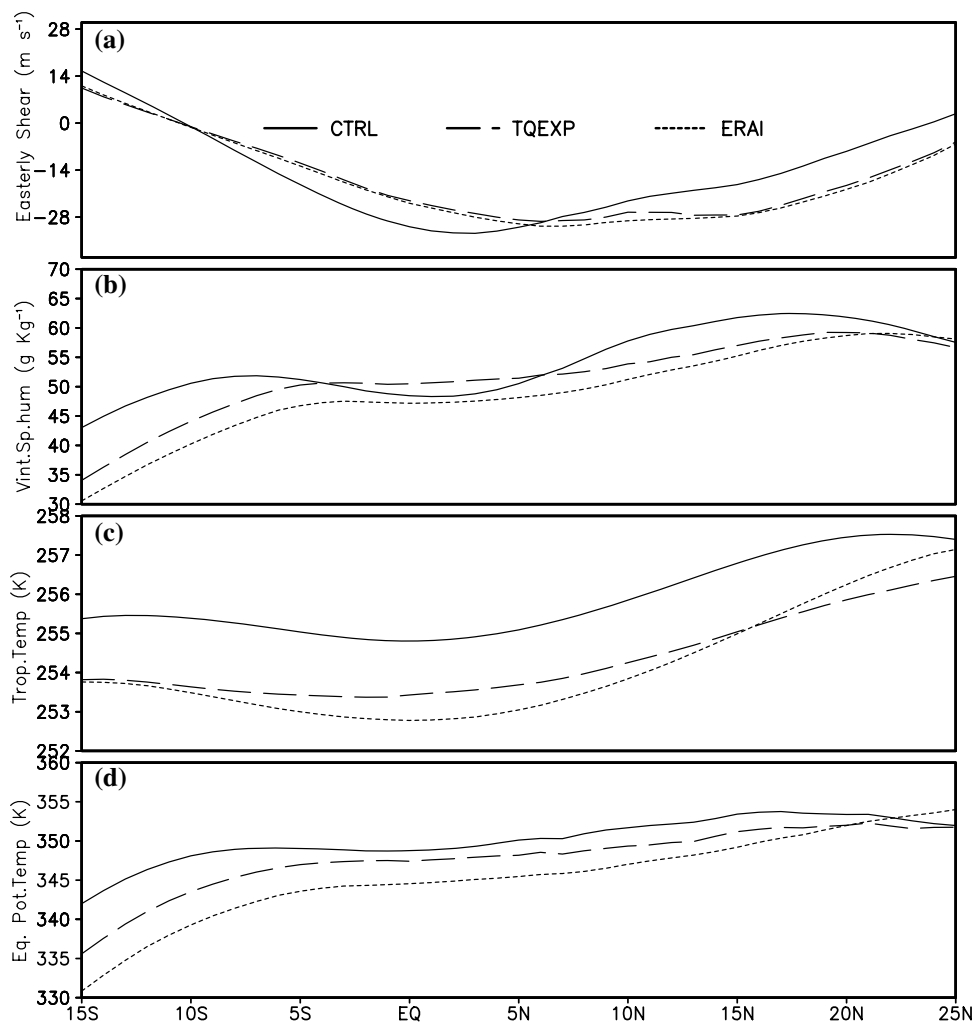
Fig. 5 JJAS mean spatial distribution of vertical wind shear of the zonal winds (U200–U850) (a–c, ms^{-1}) and JJAS mean of precipitation (d–f, mm d^{-1}) from CTRL, TQEXP and GPCP

specific humidity (Fig. 6b) is one of the prevailing features in CTRL. Another significant difference is the meridional tropospheric temperature (Fig. 6c), which is overestimated by CTRL. However in TQEXP easterly shear, gradient of specific humidity and meridional tropospheric temperature are consistent with the ERAI, this leads to better representation of lower troposphere EPT distribution (Fig. 6d).

In order to examine the diagnostics for the proper representation of moist physics due to assimilation of vertical moist and thermodynamic profiles, vertically integrated PW and MSE are studied from CTRL, TQEXP and ERAI (Fig. 7). In CTRL (Fig. 7a), PW is higher ($\geq 60 \text{ kg m}^{-2}$) over the land region along with adjacent oceanic regions.

In TQEXP (Fig. 7b) the spatial distribution of PW shows maxima over head BoB, north eastern India and MCR as in ERAI (Fig. 7c). In general, higher values of PW lead to excess MSE at lower troposphere, supporting unstable boundary layer, convective ascent and excess rainfall (e.g. Emanuel et al.1994; Sabin et al. 2013). The representation of instability in TQEXP (Fig. 7b) is consistent with ERAI whereas CTRL represents stronger instability compared to ERAI (Fig. 7a). In addition to this vertically integrated moisture transport and moisture flux divergence are examined in CTRL, TQEXP and ERAI (Fig. 8). The strongest moisture convergence is observed in BoB and South China Sea region during monsoon. CTRL (Fig. 8a) shows

Fig. 6 Seasonal mean meridional distribution of **a** easterly wind shear (ms^{-1}), **b** vertical integrated specific humidity (g Kg^{-1}), **c** tropospheric temperature (K) and **d** lower tropospheric equivalent potential temperature averaged between 65°E and 95°E from CTRL (solid line), TQEXP (long dash line) and ERAI (dotted line)



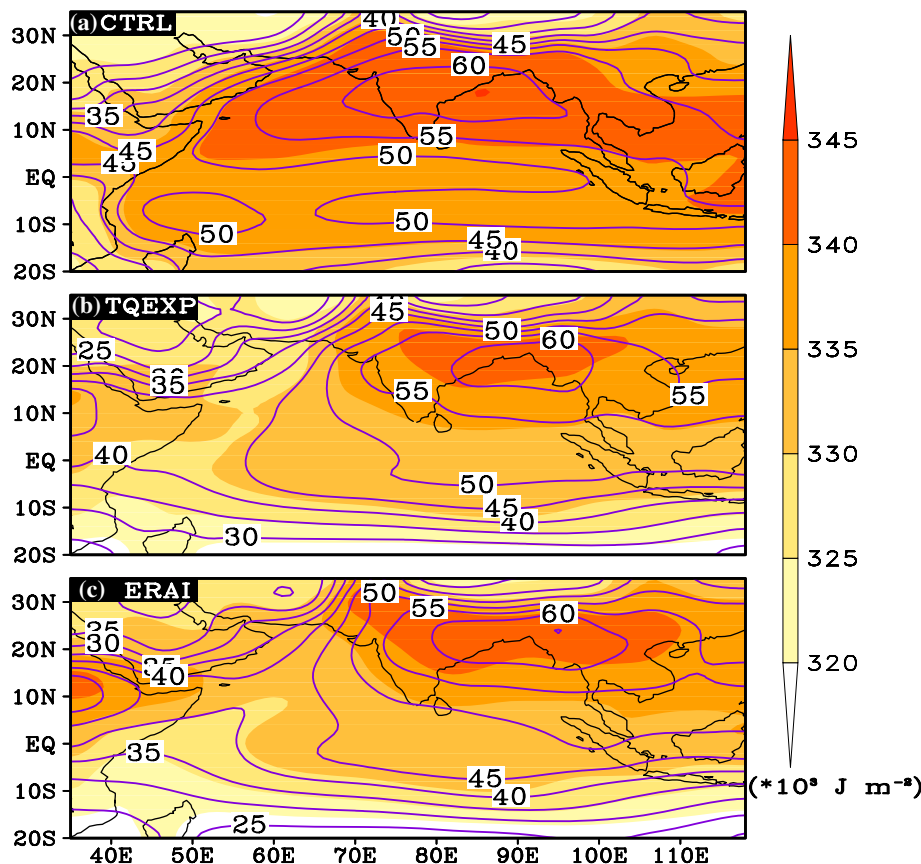
higher moisture transport all the way from AS, BoB and land region. Unrealistic convergence of moisture flux is seen over AS and along the west coast of India. TQEXP produces moisture transport similar to ERAI (Fig. 8b, c), which in turn helps to better represent of the moist dynamics and associated precipitation processes over convective regions in the model.

3.3 Temporal evolution of monsoon features over MCR

Apart from mean features, it is important to study the temporal evolution of monsoon features over the MCR. Figure 9a shows the temporal evolution of low level zonal wind averaged over the MCR. In CTRL, westerly winds are underestimated throughout the season and unrealistic easterlies are present from August onwards. In case of TQEXP, the seasonal evolution of zonal wind is westerly throughout the season and greater than 4 ms^{-1} until the second week of August and then gradually decreases as reported in ERAI with temporal correlation coefficient of 0.93 (0.86 in CTRL). In addition to the winds, the TQEXP

displayed better structure of vorticity evolution over the MCR (Fig. 9b) including peak and the withdrawal phase of the monsoon. TQEXP shows higher temporal correlation coefficient (0.9) than CTRL (0.7). Temporal evolution of tropospheric temperature in CTRL displays warm bias (1.5 K) during the entire monsoon season (Fig. 9c), however, TQEXP displays a cold bias with respect to ERAI. Vertically integrated (surface to 400 hPa) WVMR (Fig. 9d) is overestimated by CTRL, whereas TQEXP could provide the proper evolution of tropospheric water vapour throughout the season with correlation coefficient of 0.97. Thus, by assimilating AIRS profiles one could considerably improve the temporal evolution of monsoon associated fields over the MCR in the model. This may lead to a proper temporal evolution of rainfall in the model. Figure 9e shows the temporal evolution of precipitation from CTRL, TQEXP and GPCP. CTRL overestimates precipitation (7 mm d^{-1}) during the peak monsoon months (July and August). This bias can be explained by unrealistic moisture transport from BoB and the Philippine Sea by easterly winds. Lucas-Picher et al. (2011) found that such biases in precipitation over the

Fig. 7 Spatial map of total precipitable water (Kg m^{-2} ; contours) and moist static energy ($\times 10^3 \text{ J m}^{-2}$; shaded) vertically averaged from 1000 to 700 hPa from a CTRL, b TQEXP and c ERAI for JJAS



ISM region is one of the concern in many regional models. It is important to note that TQEXP could bring down the dominant positive bias of precipitation to 1.5 mm d^{-1} .

3.4 Vertical structures of dynamic and thermodynamic parameters over MCR

This section describes the vertical structures of the thermodynamic (temperature, WVMR and MSE) and dynamic (zonal, meridional winds, vorticity and divergence) parameters associated with ISM precipitation over the MCR.

3.4.1 Temperature, moisture and moist static energy

The mean vertical profiles of temperature from CTRL, TQEXP and ERAI (right panel in Fig. 10a) display similar pattern in the vertical structure. The seasonal evolution of vertical temperature anomalies is compared with rainfall over MCR (the temperature and rainfall anomalies are obtained by removing their seasonal mean). The boundary layer is warmer (1.5–2 K) in the observations during the first three weeks of June whereas the middle to upper troposphere is cooler (1–1.5 K). While during July and August, strong warming from middle to upper troposphere and the corresponding cooling in the atmospheric boundary layer

is evident in CTRL, TQEXP and ERAI, which is consistent with the precipitation variability. However, CTRL produces stronger mid tropospheric temperature anomalies than ERAI, which is consistent with the inherent wet bias induced latent heating. On the other hand, the boundary layer warm bias is due to the underestimation of evaporative cooling. TQEXP produced proper vertical thermal structure and its seasonal evolution corresponding to the rainfall over the MCR. Importantly, the baroclinic response of temperature is better portrayed in TQEXP compared to that of CTRL (weaker during July and August). FI for temperature supports the reduction in bias by 60–70% in the boundary layer and upper troposphere over the MCR.

The mean vertical structures of WVMR associated with the monsoon in CTRL and TQEXP are consistent with ERAI for the entire troposphere (Fig. 10b). However, CTRL shows a dry (wet) bias at the surface to lower troposphere (mid to upper troposphere) over MCR as compared to ERAI. FI of WVMR shows higher skill (FI of 50–70%) in the middle to upper troposphere, whereas the skill is relatively less in the surface (10%) and lower troposphere (30–40%). The WVMR anomalies in CTRL and TQEXP are negative until the third week of June and the vertical extent is up to 200 hPa, while it has strong positive anomalies during July and August. But CTRL has higher

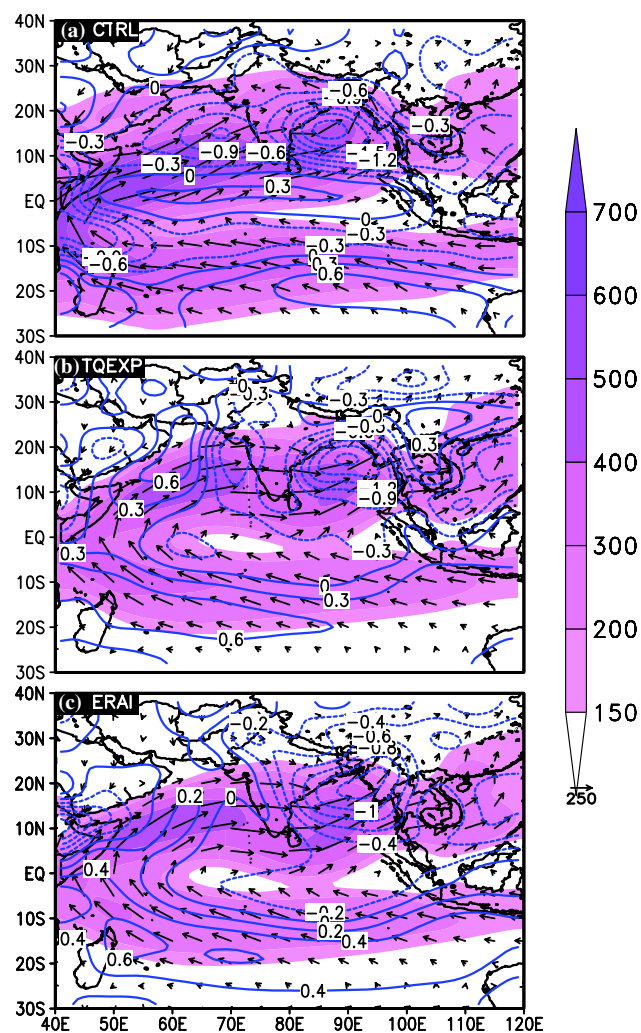


Fig. 8 JJAS mean vertically integrated moisture transport (shaded; $\text{Kg m}^{-1} \text{s}^{-1}$) and moisture flux divergence (contours; Kg s^{-1}) from a CTRL, b TQEXP and c ERAI. The arrows shows the moisture components QU and QV

WVMR with higher than observed vertical extent. Overall the CTRL displays a wet bias during the peak monsoon, on the other hand, the higher WVMR loading seen in the lower to middle troposphere is reduced in TQEXP and the vertical extent of WVMR anomalies are comparable with ERAI. Further, MSE analysis associated with monsoon rainfall processes over MCR reveals that the mean vertical structure of MSE is captured in CTRL and TQEXP (Fig. 10c). However, MSE is underestimated in the upper boundary layer to the free troposphere in CTRL (Fig. 10c) but TQEXP overestimates MSE in the lower troposphere. Observations show that MSE decreases with height in the low to mid troposphere over MCR, which is underestimated by the CTRL. This indicates that CTRL is more unstable during the convective phase in the lower to mid

troposphere, potentially pumping up moisture to the deeper extent resulting in a positive precipitation bias and higher MSE anomaly than in the observations.

3.4.2 Zonal and meridional wind

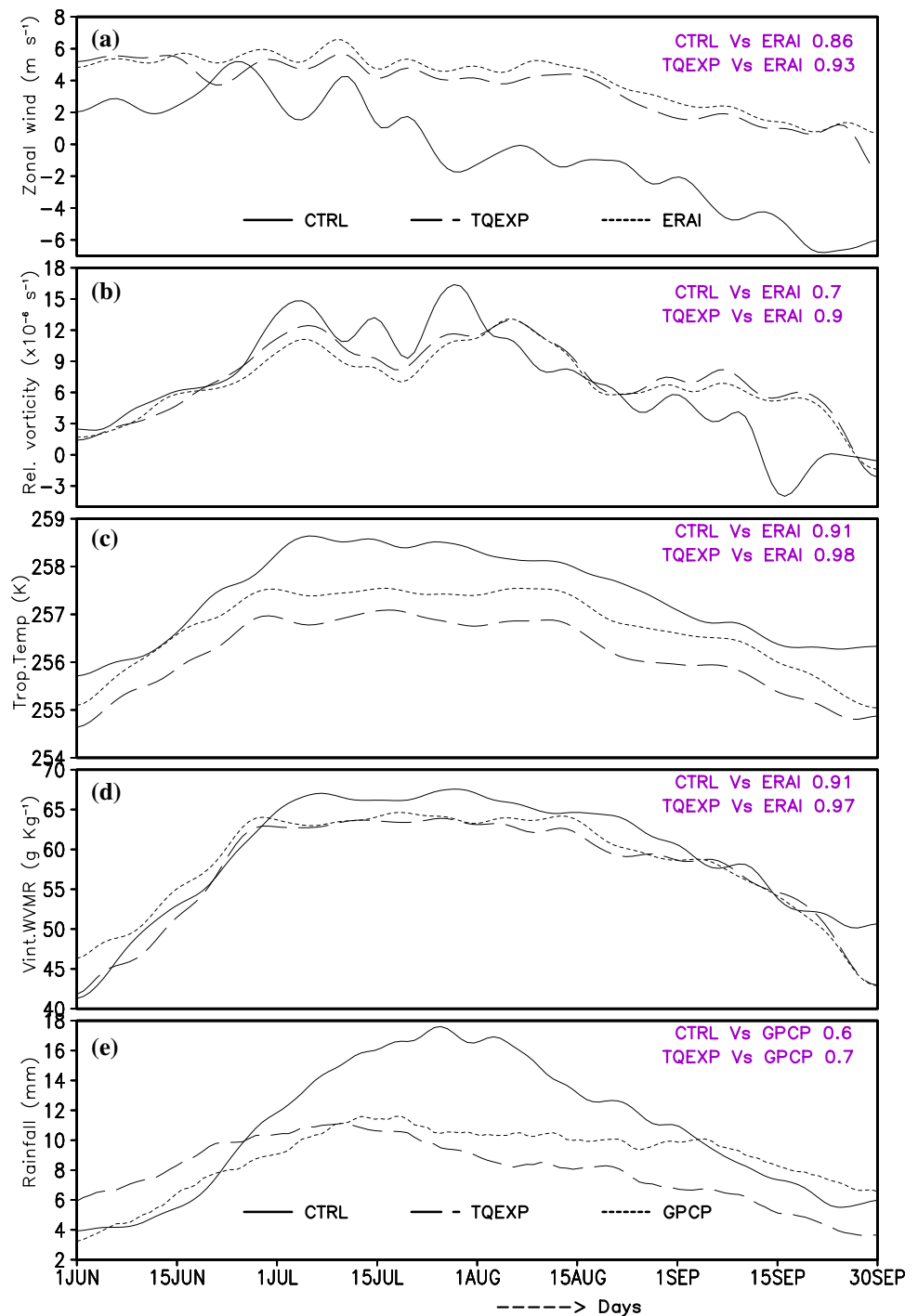
Figure 11a shows the vertical distribution of mean zonal wind and time-height cross section of zonal wind anomalies superimposed by rainfall anomalies over the MCR from CTRL, TQEXP and ERAI. CTRL displays weak westerly (easterlies) wind in the boundary layer (upper troposphere, Fig. 11a). This suggests weak mean monsoon zonal flow in the entire troposphere and weak vertical shear of zonal wind. On the other hand, TQEXP shows strong westerlies (easterlies) in the lower troposphere (upper troposphere) as in ERAI. During the withdrawal phase of the monsoon, lower tropospheric easterly anomalies and upper tropospheric westerly anomalies appeared in the CTRL and are stronger than TQEXP and ERAI. Thus, TQEXP shows quite a realistic evolution of vertical structure of zonal wind (zonal shear) over the MCR. Overall the modification in the zonal circulation in the model is (about 60–70%) obtained due to the inclusion of AIRS profiles.

Mean vertical profiles of meridional wind and time height cross section of meridional wind anomalies associated with the rainfall over MCR from CTRL, TQEXP and ERAI are shown in Fig. 11b. The time mean vertical structure of meridional wind in the CTRL displays slightly strong southerlies (weak northerlies) in the lower and upper troposphere (mid troposphere) than in ERAI. Thus, the model overestimates meridional wind shear compared to ERAI. However, the meridional wind shear in the TQEXP is more realistic than CTRL with 50–65% of FI. This enhancement in the circulation representation is consistent with Raju et al. (2015b, c) where temperature profiles from satellite observations are assimilated. Figure 11b (left panel) shows the temporal evolution of meridional wind and precipitation anomalies from the model and ERAI. CTRL shows negative wind anomalies until the end of July with a vertical extent up to 300 hPa, while the rest of the season it is positive. TQEXP displays positive wind anomalies in the lower troposphere as in ERAI till the mid August and is negative rest of the season.

3.4.3 Vorticity and divergence

CTRL underestimates cyclonic vorticity in the lower to mid troposphere even though it has excess tropospheric heating. Strong positive vorticity anomalies are evident during the peak monsoon phase, whereas negative vorticity anomalies are seen during the onset and withdrawal stages in ERAI, CTRL, and TQEXP (Fig. 11c). Moreover, these anomalies are overestimated during the peak phase of the monsoon in

Fig. 9 Temporal evolution of area averaged: **a** low level (at 850 hPa) zonal wind (ms^{-1}), **b** relative vorticity (s^{-1}), **c** tropospheric temperature (K), **d** vertical integrated WVMR (g Kg^{-1}) and **e** rainfall (mm d^{-1}) over the MCR during JJAS. CC is represented at the *top right corner*



CTRL. In contrary, strong low level cyclonic vorticity up to 500 hPa and anticyclonic vorticity aloft are evident in the TQEXP and ERAI. TQEXP produced proper seasonal evolution of both the cyclonic and anticyclonic response compared to CTRL. Mean profiles of divergence and time height cross section of its anomaly associated with rainfall anomalies are shown in Fig. 11d. Time mean divergence profiles in ERAI display strong low level convergence and mid to upper tropospheric divergence. CTRL shows slight

overestimation in the low level convergence than ERAI, while TQEXP overestimated divergence at mid troposphere. Time height cross section of anomalous divergence over MCR (corresponding to rainfall) reveals strong upper level divergence and low level convergence during the peak monsoon months in the CTRL (Fig. 11d). Low level divergence and upper level convergence anomaly during the onset and withdrawal phases of monsoon are properly produced in the TQEXP than CTRL. Hence the time evolution

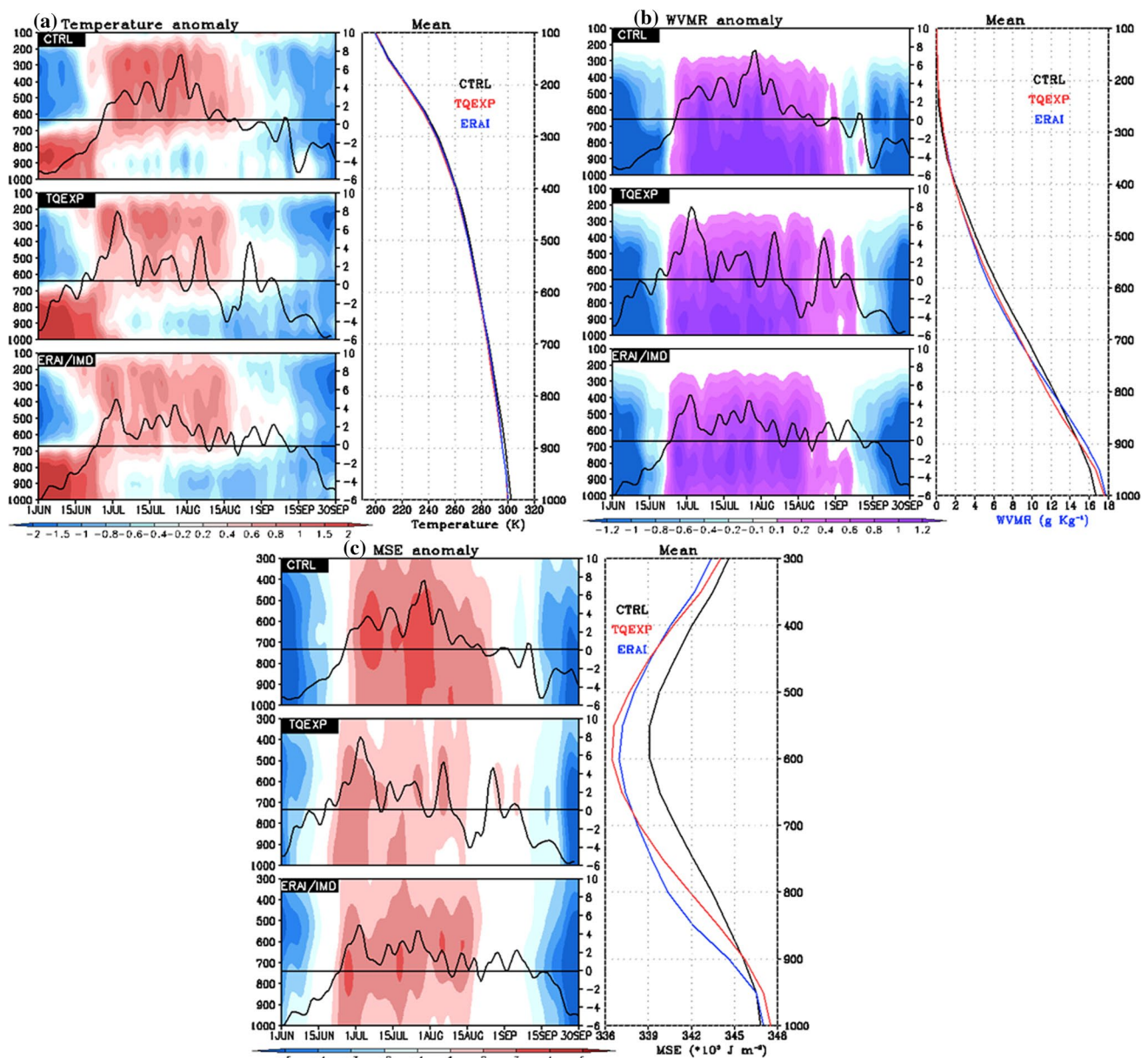


Fig. 10 Time-height cross section (JJAS) of anomaly (shaded, left panels) and mean vertical profiles (right panels) over MCR from CTRL (black), TQEXP (red) and ERAI (blue) for **a** temperature (K),

b WVMR (g Kg^{-1}) and **c** moist static energy ($\times 10^3 \text{ J m}^{-2}$). Rainfall anomaly (mm d^{-1} , solid line and scales at right) overlaid on time-height cross section (left panels)

of divergence structure is more realistic in the TQEXP. Our results corroborate that continuous assimilation of temperature and WVMR profiles can yield better representation of vorticity and divergence of monsoon circulations fields over MCR.

3.5 Assessment of moist convection over the MCR

This section assesses the longitude-height cross section of specific humidity and MSE over the MCR region (Fig. 12). In general the zonal gradient of specific humidity is positive

(higher in the east and lower in the west) and vertical extent of moisture ($>14 \text{ g Kg}^{-1}$) is higher in the east than the western flank of MCR (Fig. 12c). This east–west gradient of the specific humidity is weaker in CTRL (Fig. 12a). Nevertheless, it is noted that a sharp zonal gradient of specific humidity is evident in the TQEXP (Fig. 12b). The vertical extent of specific humidity is improved in the TQEXP. The convective instability in the MCR can be inferred from the vertical structure of MSE (e.g. Sabin et al. 2013). ERAI shows sharp zonal gradient in the MSE with higher magnitudes in the eastern flank and lower magnitudes in

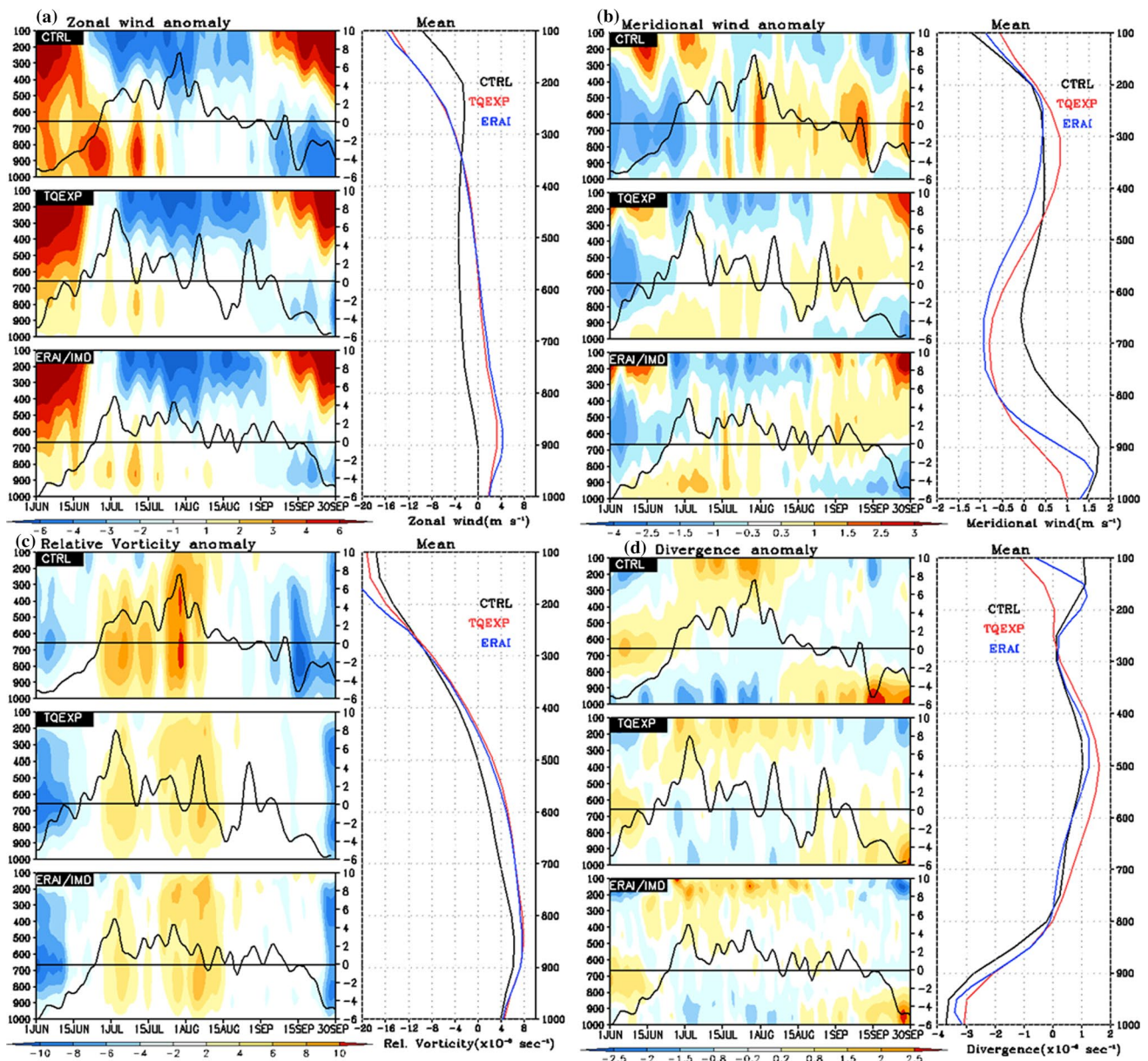


Fig. 11 Time-height cross section of anomaly (shaded, left panels) and mean vertical profiles (right panels) over MCR from CTRL (black), TQEXP (red) and ERAI (blue) for **a** zonal wind (m s^{-1}), **b** meridional wind (m s^{-1}), **c** relative vorticity ($\times 10^6 \text{ s}^{-1}$), **d** divergence

($\times 10^6 \text{ s}^{-1}$). Rainfall anomaly (mm d^{-1} , solid line and scales at right) overlaid on time-height cross section (left panels) from June to September

the western flank of the MCR (Fig. 12). This fascinating structure (strength and location) is well captured in the TQEXP whereas it is weak or absent in the CTRL. Time evolution of MSE over MCR (Fig. 12d) displays gradual increase from the monsoon onset onwards, is broadly captured by CTRL, TQEXP and ERAI. However, the amount of instability produced is higher in CTRL as compared to ERAI, while TQEXP shows moist instability similar to that of ERAI, particularly during the peak monsoon months. It is also noted that the TQEXP underestimates MSE at the

initial stage of monsoon evolution. Thus, the temporal evolution of MSE is better represented in TQEXP over MCR.

3.6 Statistical skill scores for rainfall

Previous analysis indicates that the assimilation of temperature and water vapour profiles in models had a significant impact on the thermodynamic variables associated with the ISM. Thus, it is important to verify whether these results supported by the statistical skill scores for

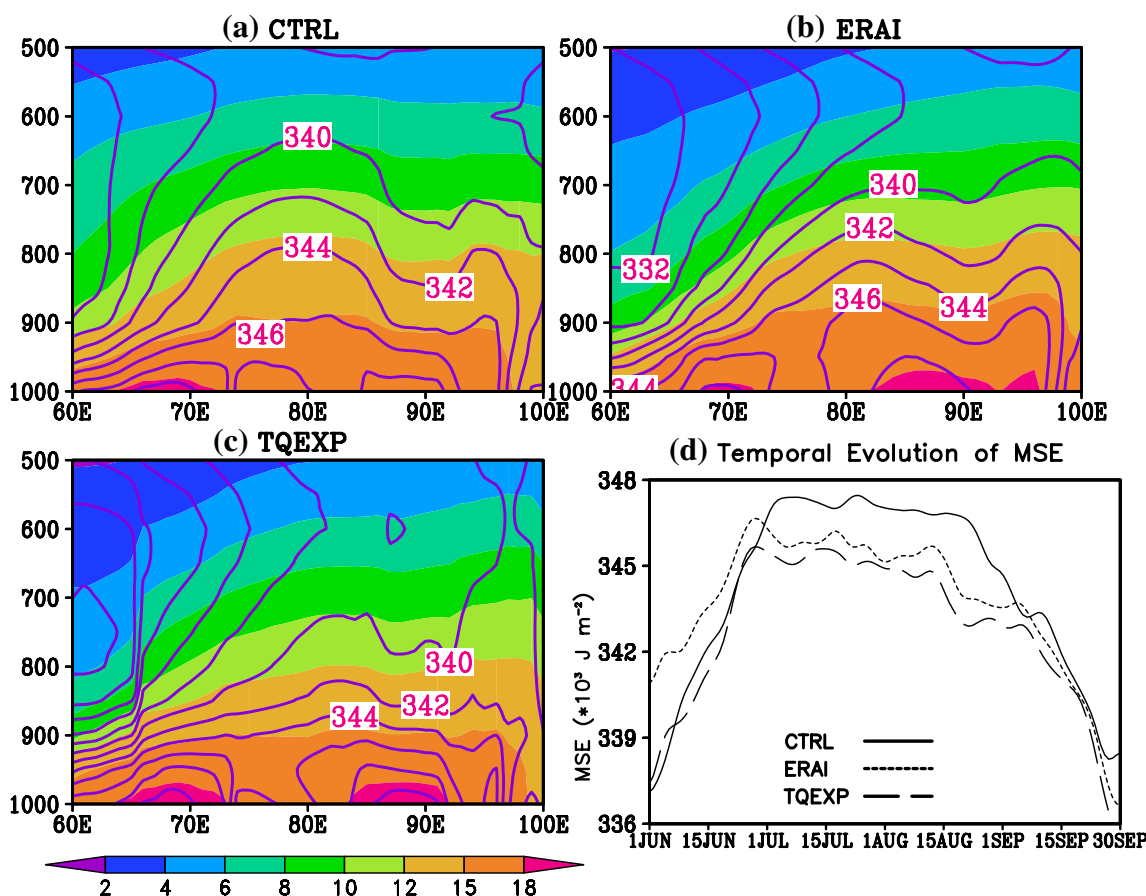


Fig. 12 Longitude-height cross section of specific humidity (g Kg^{-1} ; shaded) and moist static energy ($\times 10^3 \text{ Jm}^{-2}$; contours) averaged between 16°N and 28°N latitudes from **a** CTRL, **b** ERAI and **c** TQEXP. **d** Temporal evolution of moist static energy over MCR during monsoon

Table 2 Bias and RMSE for model daily rainfall against to TRMM observed rainfall over different regions

Experiment	Bias (mm d^{-1})				RMSE (mm d^{-1})			
	MCR	WGR	BoB	EIO	MCR	WGR	BoB	EIO
CTRL	0.72	4.8	9.2	-6.2	2.31	7.04	10.5	6.2
TQEXP	0.43	4.6	9.5	6.8	2.11	6.25	10.8	9.5

rainfall. The RMSE and bias of CTRL and TQEXP rainfall over different regions are given in Table 2. TQEXP reports lesser RMSE and bias over MCR, Western Ghat region (WGR) compared to CTRL, however RMSE over the EIO and BoB is found to be higher in TQEXP than CTRL. To examine the performance of the model in representing the frequency of rainfall occurrence events for particular precipitation threshold, BS and ETS are computed against TRMM observations based on the contingency approach (Colle et al. 1999; Wilks 2006). These statistical skill scores are computed for different thresholds such as low (<5 mm), moderate (5–20 mm) and high rainfall (>20 mm) categories, which are displayed in the Table 3. Over MCR and WGR, skill scores are better for

Table 3 Statistical skill scores (ETS and BS) for model daily mean rainfall against to TRMM observed rainfall over MCR for low, moderate and high rainfall categories

Zone	Rainfall categories	Equitable threat score (ETS)		Bias score (BS)	
		CTRL	TQEXP	CTRL	TQEXP
MCR	<5	0.14	0.16	1.22	0.78
	5–20	0.17	0.22	0.69	0.4
	>20	0.04	0.12	2.22	1.06

all type of rainfall categories in TQEXP compared to CTRL. In the case of BoB and EIO, these skill scores got better only for lower categories, but not for moderate and

high rainfall events. Thus, the rainfall analysis benefits from temperature and moisture information offered by AIRS.

4 Possible physical mechanisms

Previous section demonstrated that assimilation of AIRS profiles produces near realistic monsoon features in the downscaled products. This development is due to proper representation of the spatial and temporal coverage of temperature and moisture fields, which played a key role in the representation of the baroclinic structure of the monsoon. Secondly, continuous assimilation of temperature and moisture profiles leads to proper temporal evolution of dynamic and thermodynamic structures such as easterly wind shear, lower tropospheric specific humidity, tropospheric temperature gradient and EPT associated with the ISM. The detail analysis revealed that the discrepancies of easterly shear due to improper thermal/pressure gradients during ISM lead to misrepresentation of monsoon dynamics in CTRL. This discrepancy leads to excess moisture, the release of additional latent heat, which ultimately results in improper tropospheric temperature gradients and feedback to the monsoon circulation. While in TQEXP, a realistic thermal gradient over the monsoon domain produces proper spatial and temporal distribution of heat, moisture, circulation and its associated processes. The realistic representation of monsoon circulation helps better moisture transport resulting proper moist convective feedback. In addition to that, better representation of monsoon circulation and converging zones leads to an accurate easterly shear and moist instability structures in TQEXP. According to Krishnamurti et al. (1976b), the proper TT gradient (Fig. 6c) can lead to better reproduction of vertical easterly wind shear (Fig. 6a), which imposes the meridional extend of ISM. Reale et al. (2017) reported that the proper easterly shear can lead to more realistic convective processes and feedback to associated dynamics. This mechanism helps to improve monsoon representation at regional scale. Therefore, the present study emphasize that the incorporation of AIRS soundings is highly useful for the better representation of the monsoon system due to the systematic tropospheric thermal and moisture structure in the model, thereby, providing a good opportunity to identify the moist thermodynamic physical response in the model convective parameterization schemes.

5 Summary and concluding remarks

The study examined the impact of assimilation of AIRS temperature and water vapour profiles on the ISM in WRF

model. The assimilation of these profiles had a significant impact on the ISM representation due to their better representation of thermodynamic structure in the model. Specifically, the advantages of AIRS data ingestion are summarized as follows: it resulted in (1) the realistic representation of strength and location of monsoon elements, (2) disappearance of the unrealistic double ITCZ like rainfall pattern due to proper monsoon circulation, (3) better representation of the meridional distribution of temperature, water vapour, MSE and wind shear, (4) proper vertical structure of moisture, vorticity, divergence and vertical velocities. Further, assimilation of satellite retrieved temperature and water vapour profiles could significantly modify the moist physical processes and the associated rainfall over MCR. The ingestion of AIRS profiles enhances the realistic spatial distribution of precipitation and statistical skill scores over the land regions as compared to the skill scores in CTRL experiment. It also allowed a realistic representation of the thermal structure and its influence on the moisture convergence associated with spatial distribution of precipitation patterns (through dynamic interactions of deep convection with the atmospheric boundary layer). This further reiterates the importance of representing the heating distribution which is responsible for the accurate ISM structure in any regional model. Our results advocate that the AIRS retrievals would be of great benefit for process based studies and for the preparation of regional reanalysis in downscaling context.

Acknowledgements We thank the Director of ESSO-IITM for support. We are grateful to the anonymous reviewers for constructive comments and valuable suggestions, which have helped us to substantially improve this article. We also thank Dr. Oreste Reale for his valuable suggestions, edits and comments on our manuscript. We thank Mr. Cesar Weston and Dr. P. R. C. Reddy for language editing. The authors are grateful to NCAR, Boulder, Colorado, USA for making the WRF-ARW model available. The AIRS data used in this study are obtained from the NASA Goddard Earth Sciences (GES) Data and Information Services Center (DISC) Distributed Active Archive Center (DAAC). Authors are thankful to ECMWF for reanalysis obtained from their data server. Thanks are also due to TRMM and GPCP for providing the rainfall data used in this study. Produced downscale reanalysis in this study is presently available on request basis later it may be provided on open access.

References

- Abhik S, Mukhopadhyay P, Goswami B (2014) Evaluation of mean and intraseasonal variability of Indian summer monsoon simulation in ECHAM5: identification of possible source of bias. *Clim Dyn* 43:389–406
- Anthes RA, Kuo YH, Hsie EY, Low-Nam S, Bettge TW (1989) Estimation of skill and uncertainty in regional numerical models. *Q J R Meteorol Soc* 115:763–806
- Aumann HH, Chahine MT, Gautier C, Goldberg MD, Kalnay E, McMillin LM, Revercomb H, Rosenkranz PW, Smith WL, Staehlin DH, Strow LL, Suskind J (2003) AIRS/AMSU/HSB on the

- Aqua mission: design, science objectives, data products, and processing system. *IEEE Trans Geosci Remote Sens* 41:253–264
- Colle BA, Westrick KJ, Mass CF (1999) Evaluation of MM5 and Eta-10 precipitation forecast over the Pacific northwest during the cool season. *Weather Forecast* 14:137–154
- Cressman GP (1959) An operational objective analysis system. *Mon Wea Rev* 87:367–374
- Davolio S, Buzzi A (2004) A Nudging scheme for the assimilation of precipitation data into a mesoscale model. *Weather Forecast* 19:855–871
- Dee DP, Uppala SM, Simmons AJ, Berrisford P, Poli P, Kobayashi S, Andrae U, et al (2011) The ERA-Interim reanalysis: configuration and performance of the data assimilation system. *Q J R Meteorol Soc* 137:553–597
- Divakarla MG, Barnett CD, Goldberg MD, McMillin LM, Maddy E, Wolf W, Zhou L, Liu X (2006) Validation of Atmospheric Infrared Sounder temperature and water vapor retrievals with matched radiosonde measurements and forecasts. *J Geophys Res*. doi:10.1029/2005JD006116
- Emanuel KA, Neelin JD, Bretherton CS (1994) On large-scale circulations in convective atmospheres. *Q J R Meteorol Soc* 120:1111–1143
- Fan X, Tilley SJ (2005) Dynamic assimilation of MODIS-retrieved humidity profiles within a regional model for high-latitude forecast applications. *Mon Weather Rev* 133:3450–3480
- Fast JD (1995) Mesoscale modeling and four-dimensional data assimilation in areas of highly complex terrain. *J Appl Meteorol* 34:2762–2782
- Fu XH, Wang B, Tao L (2006) Satellite data reveal the 3-D moisture structure of tropical intraseasonal oscillation and its coupling with underlying ocean. *Geophys Res Lett* 33:L03705. doi:10.1029/2005GL025074
- Gadgil S, Gadgil S (2006) The Indian monsoon, GDP and agriculture. *Econ Polit Wkly* 41:4887–4895
- Huffman GJ, Adler RF, Morrissey M, Bolvin DT, Curtis S, Joyce R, McGavock B, Susskind J (2001) Global precipitation at one-degree daily resolution from multi-satellite observations. *J Hydrometeorol* 2:36–50. doi:10.1175/1525-7541(2001)002<0036:GPAODD>
- Huffman GJ, Adler RF, Bolvin DT, Gu G, Nelkin EJ, Bowman KP, Hong Y, Stocker EF, Wolff DB (2007) The TRMM multisatellite precipitation analysis (TMPA): quasi-global, multiyear, combined-sensor precipitation estimates at fine scales. *J Hydrometeorol* 8:38–55
- Jiang X, Li T, Wang B (2004) Structures and mechanisms of the northward propagating boreal summer intraseasonal oscillation. *J Clim* 17:1022–1039
- Joseph PV, Sijkumar S (2004) Intraseasonal variability of the low-level jet stream of the Asian summer monsoon. *J Clim* 17:1449–1458
- Krishnamurti TN, Bhalme HN (1976a) Oscillations of a monsoon system, part I: observational aspects. *J Atmos Sci* 33:1937–1954
- Krishnamurti TN, Molinari J, Pan HL (1976b) Numerical simulation of the Somali jet. *J Atmos Sci* 33:2350–2362
- Krishnamurti TN, Cunningham P, Rajendran K (2005) Anomalous gradient winds in the subtropical jet stream and interpretations of forecast failures. *Meteorol Atmos Phys* 88:237–250. doi:10.1007/s00703-004-0075-x
- Lakshminarayanan S, Lewis JM (2011) When is nudging optimal. Technical report, School of Computer Science, University of Oklahoma, Norman, 73019
- Lau K-M, Kim K-M, Yang S (2000) Dynamical and boundary forcing characteristics of regional components of the Asian summer monsoon. *J Clim* 13:2461–2482
- Le Marshall J et al (2006) Improving global analysis and forecasting with AIRS. *Bull Am Meteorol Soc* 87:891–894
- Leslie LM, LeMarshall JF, Morrison RP, Spinoso C, Purser RJ, Pescod N, Seecamp R (1998) Improved hurricane track forecasting from the continuous assimilation of high quality satellite wind data. *Mon Weather Rev* 126:1248–1257
- Li J, Liu H (2009) Improved hurricane track and intensity forecast using single field-of-view advanced IR sounding measurements. *Geophys Res Lett* 36:L11813. doi:10.1029/2009GL038285
- Liang X-Z, Xu M, Yuan X, Ling T, Choi HI, Zhang F, Chen L, Liu S, Su S, Qiao F, He Y, Wang JXL, Kunkel KE, Gao W, Joseph E, Morris V, Yu T-W, Dudhia J, Michalakes J (2012) Regional climate-weather research and forecasting model (CWRF). *Bull Am Meteorol Soc*. doi:10.1175/BAMS-D-11-00180.1
- Lin R, Zhou T, Qian Y (2014) Evaluation of global monsoon precipitation changes based on five reanalysis datasets. *J Clim* 27(3):1271–1289
- Lucas-Picher P, Christensen JH, Saeed F, Kumar P, Asharaf S, Ahrens B, Wiltshire AJ, Jacob D, Hagemann S (2011) Can regional climate models represent the Indian monsoon? *J Hydrometeorol* 12(5):849–868. doi:10.1175/2011jhm1327.1
- McNally AP, Watts PD (2003) A cloud detection algorithm for high-spectral-resolution infrared sounders. *Q J R Meteorol Soc* 129:3411–3423. doi:10.1256/qj.02.208
- Miyoshi T, Kunii M (2012) Using AIRS retrievals in the WRF-LETKF system to improve regional numerical weather prediction. *Tellus A* 64:18408. doi:10.3402/tellusa.v64i0.18408
- Otkin JA (2012) Assimilation of water vapor sensitive infrared brightness temperature observations during a high impact weather event. *J Geophys Res* 117:D19203. doi:10.1029/2012JD017568
- Parkinson CL (2003) Aqua: an Earth-observing satellite mission to examine water and other climate variables. *IEEE Trans Geosci Remote Sens* 41:173–183
- Raju A, Parekh A, Chowdary JS, Gnanaseelan C (2014) Impact of satellite retrieved atmospheric temperature profiles assimilation on Asian summer monsoon simulation. *Theor Appl Climatol* 116:317–326
- Raju A, Parekh A, Chowdary JS, Gnanaseelan C (2015a) Assessment of the Indian summer monsoon in the WRF regional climate model. *Clim Dyn* 44:3077–3100. doi:10.1007/s00382-014-2295-1
- Raju A, Parekh A, Kumar P, Gnanaseelan C (2015b) Evaluation of the impact of AIRS profiles on prediction of Indian summer monsoon using WRF variational data assimilation system. *J Geophys Res Atmos* 120:8112–8131. doi:10.1002/2014JD023024
- Raju A, Parekh A, Sreenivas P, Chowdary JS, and Gnanaseelan C (2015c) Estimation of improvement in Indian summer monsoon circulation by assimilation of temperature profiles in WRF model. *IEEE J Sel Top Appl Earth Obs Remote Sens*. doi:10.1109/JSTARS.2015.2410338
- Rakesh V, Singh R, Joshi PC (2010) Impact of four dimensional assimilation of satellite data on long-range simulations over the Indian region during monsoon 2010. *Adv Space Res* 46:895–908
- Raymond WH, Wade GS, Zapotocny TH (2004) Assimilating GOES brightness temperatures. Part I: upper-tropospheric moisture. *J Appl Meteorol* 43:17–27
- Reale O, Lau KM, Susskind J, Rosenberg R (2012) AIRS impact on analysis and forecast of an extreme rainfall event (Indus River Valley, Pakistan, 2010) with a global data assimilation and forecast system. *J Geophys Res* 117:D08103. doi:10.1029/2011JD017093
- Reale O, Achuthavarier D, Fuentes M, Putman W, Partyka G (2017) Tropical cyclone in the 7-km NASA nature run for use in observing system simulation experiments. *J Atmos Oceanic Technol* 34:73–100. doi:10.1175/JTECH-D-16-0094.1
- Sabin TP, Krishnan R, Ghattas J, Denvil S, Dufresne J-F, Hourdin F, Pascal T (2013) High resolution simulation of the South Asian

- monsoon using a variable resolution global climate model. *Clim Dyn* 41:173–194
- Seaman NL, Stauffer DR, Lario-Gibbs AM (1995) A multiscale four-dimensional data assimilation system applied in the San Joaquin Valley during SARMAP. Part I: modeling design and basic performance characteristics. *J Appl Meteorol* 34:1739–1761
- Singh R, Pal PK, Kishtawal CM, Joshi PC (2008) Impact of Atmospheric Infrared Sounder data on the numerical simulation of a historical Mumbai rain event. *Weather Forecast* 23:892–913
- Singh R, Pal PK, Joshi PC (2010) Assimilation of Kalpana very high resolution radiometer water vapor channel radiances into a mesoscale model. *J Geophys Res* 115:D18124. doi:10.1029/2010JD014027
- Singh R, Kishtawal CM, Ojha SP, Pal PK (2012) Impact of assimilation of Atmospheric InfraRed Sounder (AIRS) radiances and retrievals in the WRF 3D-Var assimilation system. *J Geophys Res* 117:D11107. doi:10.1029/2011JD017367
- Skamarock WC, Klemp JB, Dudhia J, Gill DO, Barker DM, Duda MG, Huang XY, Wang W, Powers JG (2008) A description of the Advanced Research WRF Version 3. NCAR/TN-475 STR; NCAR Technical Note, Mesoscale and Microscale Meteorology Division, National Center of Atmospheric Research, pp. 113
- Stauffer DR, Seaman NL (1990) Use of four-dimensional data assimilation in a limited-area mesoscale model. Part I: experiments with synoptic-scale data. *Mon Weather Rev* 118:1250–1277
- Stauffer DR, Seaman NL (1994) Multiscale four-dimensional data assimilation. *J Appl Meteorol* 33:416–434
- Stauffer DR, Seaman NL, Binkowski FS (1991) Use of four dimensional data assimilation in a limited area mesoscale model. Part II: effects of data assimilation within the planetary boundary layer. *Mon Weather Rev* 119:734–754
- Susskind J, Reale O (2009) Improving forecast skill by assimilation of quality controlled AIRS Version 5 temperature soundings. In: *Proc SPIE int symp infrared spaceborne remote sensing instrum XVII*, vol 743. San Diego, p 74350G
- Susskind J, Barnett C, Blaisdell J (2003) Retrieval of atmospheric and surface parameters from AIRS/ AMSU/HSB under cloudy conditions. *IEEE Trans Geosci Remote Sens* 41:390–409
- Susskind J, Barnett C, Blaisdell J, Iredell L, Keita F, Kouvaris L, Molnar G, Chahine M (2006) Accuracy of geophysical parameters derived from Atmospheric Infrared Sounder/advanced microwave sounding unit as a function of fractional cloud cover. *J Geophys Res* 111:D09S17. doi:10.1029/2005JD006272
- Thiebaut J, Rogers E, Wang W, Katz B (2003) A new high resolution blended real-time global sea surface temperature analysis. *Bull Am Meteor Soc* 84:645–656
- Tian B, Waliser DE, Fetzer EJ, Lambrigtsen BH, Yung YL, Wang B (2006) Vertical moist thermodynamic structure and spatial-temporal evolution of the MJO in AIRS observations. *J Atmos Sci* 63:2462–2485
- Tobin DC, Revercomb HE, Knuteson RO, Lesht BM, Strow LL, Hannon SE, Feltz WF, Moy LA, Fetzer EJ, Cress TS (2006) Atmospheric radiation measurement site atmospheric state best estimates for Atmospheric Infrared Sounder temperature and water vapor retrieval validation. *J Geophys Res* 111:D09S14. doi:10.1029/2005JD006103
- Wilks D (2006) *Statistical methods in the atmospheric sciences: an introduction*, 2nd edn. Academic Press, Cambridge
- Wong S, Fetzer EJ, Tian B, Lambrigtsen B (2011) The apparent water vapor sinks and heat sources associated with the intraseasonal oscillation of the Indian summer monsoon. *J Clim* 24:4466–4479
- Xavier PK, Marzin C, Goswami BN (2007) An objective definition of the Indian summer monsoon season and a new perspective on ENSO-monsoon relationship. *Q J Meteorol Soc* 133:749–764
- Xavier VF, Chandrasekar A, Rahman H, Niyogi D, and Alapaty K (2008) The effect of satellite and conventional meteorological data assimilation on the mesoscale modeling of monsoon depressions over India. *Meteorol Atmos Phys* 101:65–92
- Zavodsky BT, Chou S, Jedlovec GJ (2012) Improved regional analyses and heavy precipitation forecasts with assimilation of Atmospheric Infrared Sounder retrieved thermodynamic profiles. *IEEE Trans Geosci Remote Sens* 50(11):4243–4251
- Zhou YP, Lau KM, Reale O, Rosenberg R (2010) AIRS impact on precipitation analysis and forecast of tropical cyclones in a global data assimilation and forecast system. *Geophys Res Lett* 37:L02806. doi:10.1029/2009GL041494